ARTICLES

Nucleon knockout from polarized ^{3}He by polarized protons at 290 MeV

A. Rahav,[1] O. Häusser,[1,2] R. M. Woloshyn,[2] T. E. Chupp,[3] P. P. J. Delheij,[2] K. Ferguson,[2] R. Henderson,[2] K. P. Jackson,[2] C. D. P. Levy,[2] J. Mildenberger,[1,*] C. A. Miller,[2] B. Morrissette,[2] and M. C. Vetterli[2]

[1]*Simon Fraser University, Burnaby, British Columbia, Canada V5A 1S6*

[2]*TRIUMF, 4004 Wesbrook Mall, Vancouver, British Columbia, Canada V6T 2A3*

[3]*The Physics Laboratories, Harvard University, Cambridge, Massachusetts 02138*

(Received 25 February 1992)

The $^3\vec{\text{He}}(\vec{p},2p)$ and $^3\vec{\text{He}}(\vec{p},pn)$ knockout reactions were observed in quasielastic kinematics at 290 MeV. Spin observables A_{n0}, A_{0n}, and A_{nn} were obtained for both reactions. Calculations using the plane wave impulse approximation (PWIA) and the free nucleon-nucleon scattering amplitudes were performed and compared with the data. The proton knockout data are in qualitative agreement with the calculations which predict A_{nn} to be sensitive to the presence of mixed-symmetry S' components in the ^{3}He wave function. Proton spins are expected to be exactly paired at momenta $q \approx 80$ MeV/c, in agreement with the A_{nn} data. Spin observables A_{0n} and A_{nn} for the $^3\vec{\text{He}}(\vec{p},pn)$ reaction deviate significantly from the PWIA predictions. The qualitative differences between proton and neutron knockout results may be caused by final-state interaction effects.

PACS number(s): 25.10.+s, 24.70.+s, 25.40.−h

I. INTRODUCTION

In recent years polarized targets with significant polarization and density have been developed at several laboratories for use in nuclear physics experiments. Since, in first order, the relative magnitude of spin-dependent effects is expected to behave like $1/A$, ^{3}He provides the best opportunity to observe spin dependence in scatterings from a dense nucleus. In this paper we report the results of an experiment carried out at TRIUMF with a polarized ^{3}He target developed jointly by TRIUMF and Simon Fraser University. We observed, for the first time, spin observables for a knockout reaction from a polarized target which, in the framework of the plane-wave impulse approximation (PWIA), provide evidence for effects of spin-momentum distributions of nucleons in the polarized target nucleus. Brief reports of this work have already appeared elsewhere [1]. These new data test our present understanding of nucleon-induced reactions at intermediate energies and of the nuclear structure of ^{3}He. This is important not just from the point of view of nuclear physics at intermediate energies, but also because of the interest and increasing feasibility in using polarized ^{3}He as a substitute for a polarized neutron target in other experiments.

The angular momentum properties of ^{3}He are such that the spin is carried mainly by the neutron, while the two protons are paired in a ($^1S_0$, $T=1$) state [2]. Consequently, nuclear reactions that involve the neutron in polarized ^{3}He can be thought of as reactions with a polarized neutron, and several experiments propose to measure the neutron-spin properties using a polarized ^{3}He target, including quasielastic [3] and deep inelastic scattering. However, before these experiments can be interpreted quantitatively, extensive theoretical and experimental work is still needed to understand implications of the spin-momentum distributions of nucleons in the ^{3}He nucleus.

In the following section we describe PWIA calculations which predict spin observables for the knockout reactions ^{3}He$(p,pn)pp$ and ^{3}He$(p,2p)^{pn}_d$. The calculations make use of Faddeev wave functions [4] for ^{3}He, of free-nucleon amplitudes [5] and of a closure approximation for the residual final states. The theoretical section will be followed by sections describing the experimental setup and the data analysis procedures. We conclude with a discussion of final results.

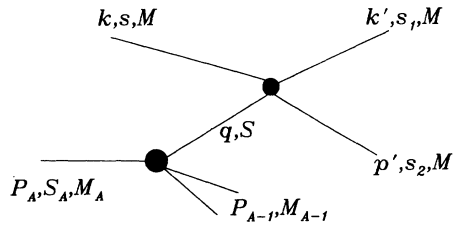

FIG. 1. Definition of momenta, spins, and masses for the PWIA calculation.

*Present address: Department of Physics, Carleton University, Ottawa, Ontario, Canada K1S 5B6.

II. PWIA ANALYSIS

We begin with a formulation of the PWIA calculations for cross sections and spin observables for the ^{3}He$(p,2p)pn$ and ^{3}He$(p,pn)pp$ reactions. In the range of momenta of the struck nucleon which is investigated here, $q<160$ MeV/c, there is experimental evidence which may suggest the validity of the PWIA. For such low nucleon momenta, the spectral functions deduced from PWIA analyses of ^{3}He$(p,2p)$ [6] and ^{3}He$(e,e'p)$ [7] reactions agree quite well with each other and with those from Faddeev calculations [4]. However, there are as yet no data on spin observables in the $A=3$ system that would allow stringent experimental tests of the reliability of the PWIA. We will show that, provided rescattering corrections turn out to be small and calculable, a comparison of the target-related spin observables with those for the elementary NN scattering at the equivalent four-momentum transfer probes directly the alignment of the spin of the struck nucleon relative to the spin of the target.

With the kinematics of Fig. 1, the cross section for nucleon knockout from nucleus A can be written [8,9] as

$$d\sigma(s,S_A)=\frac{M^4M_A}{(2\pi)^2FE}\frac{d^3k'}{E(k')}\frac{d^3p'}{E(p')}d^3P_{A-1}\sum_{\text{final states}}\delta^4(P_f-P_i)\left|\sum_S \mathcal{M}_{NN}(q,S)g_{A-1,A}(q,S)\right|^2 , \tag{1}$$

where F is the flux factor, E and q are the energy and momentum of the struck nucleon prior to the collision, and P_{A-1} is the total momentum of the residual nucleus. The sum over final states includes all final-state quantum numbers not otherwise indicated. The quantity $g_{A-1,A}(q,S)$ is the probability amplitude for finding a nucleon in a plane-wave state of momentum q and spin S with the rest of the nucleus in a state S_{A-1} and invariant mass M_{A-1}:

$$g_{A-1,A}(q,S)=\langle q,S;\phi_{A-1}(M_{A-1}),S_{A-1}|\psi_A\rangle . \tag{2}$$

The scattering of the nucleons in Eq. (1) is described by the invariant nucleon-nucleon scattering amplitude

$$\mathcal{M}=\bar{u}(p',s'_2)\bar{u}(k',s'_1)\mathcal{T}u(p,S)u(k,s) , \tag{3}$$

where $\mathcal{T}$ is the t matrix expanded in the usual S,P,T,A,V invariants. The momentum P_{A-1} can be constrained using the momentum δ function, and in the laboratory frame we have

$$\frac{d^3\sigma(s,S_A)}{d\Omega_{k'}d\Omega_{P'}d\omega}=\int\frac{M^4k'p'^2dp'}{(2\pi)^2|\mathbf{k}|EE(p')}\sum_{\text{final states}}\delta(E(k)+M_A-E(k')-E(p')-\varepsilon_{P_{A-1}})\left|\sum_S \mathcal{M}_{NN}(q,S)g_{A-1,A}(q,S)\right|^2 , \tag{4}$$

where $E(k)=(\mathbf{k}^2+M^2)^{1/2}$, etc.

To simplify the calculation, closure approximation is used to perform the sum over final states. Experimentally, the missing-mass resolution was insufficient to resolve individual final states (see next section). It is assumed that the distribution of final invariant masses M_{A-1} is sufficiently narrow that the energy in the energy δ function can be replaced by $\epsilon_{P_{A-1}}=\{P_{A-1}^2+\bar{M}_{A-1}^2\}^{1/2}$, where $\bar{M}_{A-1}$ is a suitably chosen average invariant mass. With this simplification,

$$\frac{d^3\sigma(s,S_A)}{d\Omega_{k'}d\Omega_{P'}d\omega}=\int\frac{M^4k'p'^2dp'}{(2\pi)^2|\mathbf{k}|EE(P')}\delta(E(k)+M_A-E(k')-E(p')-\{P_{A-1}^2+\bar{M}_{A-1}^2\}^{1/2})$$
$$\times\sum_{s'_1,s'_2}\sum_{S,S'}\mathcal{M}^{\dagger}_{NN}(q,S')\mathcal{M}_{NN}(q,S)D^{SS'}(q) , \tag{5}$$

where the "spin-momentum distribution"

$$D^{SS'}(q)=\sum_{(A-1)\text{ final states}}g^{\dagger}_{A-1,A}(q,S')g_{A-1,A}(q,S) \tag{6}$$

depends only on the target wave function. $D^{SS'}(q)$ can be summed to give the momentum-density distribution $\rho(q)$, i.e., $\rho(q)=\frac{1}{2}\sum_S D^{SS'}(q)$.

The spin-dependent cross section can be expressed in terms of the usual spin observables. For a spin-$\frac{1}{2}$ beam and target with polarization normal to the scattering plane,

$$\sigma(s,S_A)=\sigma_0(1+sA_{n0}+S_AA_{0n}+sS_AA_{nn}) , \tag{7}$$

where s and S_A are the polarizations of beam and target, respectively, and σ_0 is the unpolarized cross section.

In the calculations the nucleon-nucleon amplitude was constructed from the SAID [5] SM86 phase shift solution. For the special case of struck nucleons at rest, nearly on-shell NN amplitudes are involved.

The spin-dependent momentum distribution was constructed from the Afnan-Birrell [4] ^{3}He wave function as discussed in Ref. [9]. The invariant mass of the residual nucleus $\bar{M}_2$ was fixed at twice the nucleon mass.

III. EXPERIMENTAL SETUP

The experiment was carried out with the $E=290$ MeV polarized proton beam from the TRIUMF cyclotron. The experimental setup consisted of the polarized ^{3}He target, the Medium Resolution Spectrometer (MRS), and two arrays of plastic scintillators (see Fig. 2). The MRS

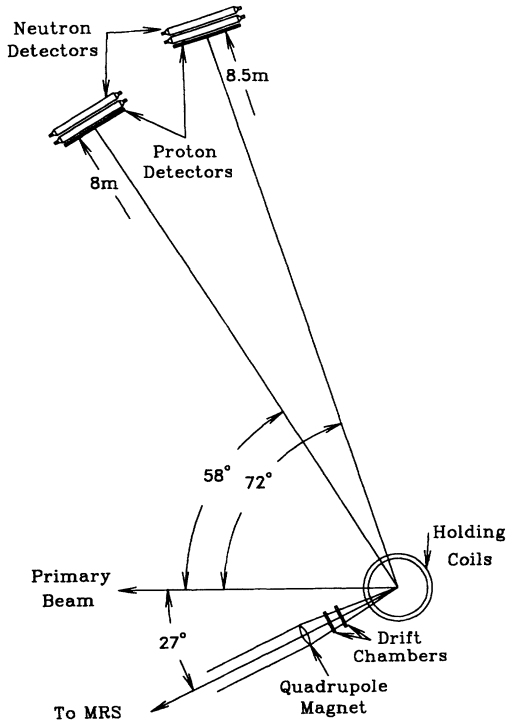

FIG. 2. Experimental setup.

was positioned at 27.5° to the left of the beam to detect and identify leading protons with energy transfers 50 MeV $<\omega=E-E'<120$ MeV. Two sets of horizontal drift chambers between the target and the MRS provided tracking to the target with <1 mm spatial resolution. This was adequate to separate events originating in both entry and exit windows of the target cell. The lower-energy final-state nucleons from the $(p,2p)$ and (p,pn) knockout reactions were measured simultaneously in two scintillator arrays located about 8 m from the target to the right of the beam at angles of 58° and 71°, respectively. Each array had an active area of 1 m^2 and consisted of a 0.6-cm-thick hodoscope followed by two 15-cm-thick scintillator layers. The thin hodoscope scintillators were used to identify neutrons and protons. Time-of-flight and energy-loss information was obtained from both thin and thick scintillators for protons and from the thick scintillators alone for neutrons. Output signals from the thick scintillators were chained together for odd and even scintillators, respectively, where individual outputs in the chain had different delays, allowing identification of the individual bar by the top-bottom delay difference. The ranges of initial momenta for the struck, identified final-state protons and neutrons were 0–110 MeV/c for the 58° array and 70–160 MeV/c for the 71° array. A custom-made ^{4}He balloon was inserted in the right-hand side between the target and scintillators to minimize multiple scattering of the lower-energy protons. Neutron bar signals were adjusted with an Am-Be source to account for the low-neutron-energy deposit. The neutron threshold was 2 MeV electron equivalent, corresponding to typical efficiencies of 10%–20% for neutron energies of 40–110 MeV [10]. The trigger for good events was defined by hardware coincidence of both the MRS (leading proton) and a hit in any of the right-hand-side scintillators.

The experiment provided the first test of a new laser-pumped ^{3}He target developed at TRIUMF. Major advances in producing ^{3}He-gas targets of sufficient density and polarization have been achieved during the past four years, with a 100-fold increase in the relevant product of areal density times polarization squared [11]. The target is based on the principle of optical pumping of Rb vapor and spin-exchange collisions with ^{3}He gas, as developed by Chupp *et al.* [12]. At a temperature of 273 K, the cell contained ^{3}He gas at 2400 Torr and N_2 gas at 100 Torr to quench fluorescence from the $^1P_{1/2}$ excited state of Rb. The target (see Fig. 1 in Ref. [1]) was designed for polarization normal to the scattering plane, had a volume of 17 cm^3, and contained 1.7×10^{21} ^{3}He atoms. At an elevated temperature of 453 K Rb vapor of density $\approx4\times10^{14}$ atoms/cm^3 was optically pumped by absorption of 4 W of circularly polarized $D1$ (795 nm) photons from a Ti:sapphire (Ti^{3+}:Al_2O_3) laser. The atomic polarization is transferred from Rb atoms to the ^{3}He nucleus during Rb-^{3}He collisions. The bulk ^{3}He polarization was reversed and analyzed using the technique of adiabatic fast-passage (AFP) NMR. Because of the weakness of the contact interaction involved [12], very low spin-exchange rates $\gamma_{SE}\approx(8\text{ h})^{-1}$ are encountered. A wall relaxation time of 43 h was measured repeatedly. The average polarization produced by this method was 54% as estimated from the relative NMR signals from ^{3}He and from water cells, at the same NMR frequency of 100 kHz. With optimized laser illumination, the maximum ^{3}He polarization was about 65%. The polarization is consistent with estimates which take into account measured spin-exchange and wall-relaxation rates and light losses from nonuniform illumination of the cell. This method has since been checked [13] by measuring the beam-related asymmetry R for the $^3\vec{\text{He}}(\vec{p},\pi^+)^4$He reaction. Strong interaction symmetries imply $A_{nn}=1$ and $A=A_{n0}=A_{0n}$ at all energies and angles [14]. After determining A with an unpolarized beam, the unknown target polarization can be extracted from a single measurement of R. Good agreement with the assumed AFP NMR value for the ^{3}He bulk polarization was obtained. The adopted "safe" error of $\Delta P_T/P_T\approx0.1$ for the target polarization is about twice as large as the value indicated by the reproducibility of the AFP NMR calibrations.

The polarized proton beam of 290 MeV had a spot size at the target of 2 mm. The ^{3}He target cell had an inner diameter of 1.6 cm and was large enough to avoid scattering from the cylindrical walls of the target. Beam polarization was changed in a 3:3:1 min sequence for the up/down/off polarization states, respectively, while target polarization was flipped every 4–6 h on the average. The average flux of protons incident on the target was about 2×10^{10} protons/sec.

IV. DATA ANALYSIS

A. Data reduction and background

Several software filters were applied to the accumulated data, supplementing the hardware requirements dis-

cussed above, to extract a background free subset of events. In this subsection those cuts are described in detail.

Particle identification on the left-hand side (leading protons) was achieved by a combined test, using the energy deposit in the MRS paddles and the time of flight from the front-end scintillator to those paddles. The trajectory length in the MRS (10.5 m) and the detector thickness ensured good separation of those protons from other particles, especially protons coming from the next beam burst. Application of this test rejected $\approx 5\%$ of the total database. Events with missing or multiple hits in any of the MRS wire chambers were rejected as well, as those events do not allow proper trajectory reconstruction and momentum analysis; they amounted to $\approx 26\%$ of the database. A gate on the calculated focal plane angle (corrected for the momentum) was used to ensure consistency of all the wire chambers coordinates (see Fig. 3).

Major sources of background events were the glass cell entry and exit windows ($\approx 140\ \mu$m thick each). The windows contained more atoms/cm^2 than the ^{3}He gas in the cell. Accurate traceback was therefore necessary in order to verify the spatial origin of the reaction. Because of the limited acceptance of the MRS and its tendency to decrease sharply from the target center, the ratio of glass events to ^{3}He events was considerably reduced. In Fig. 4 both the vertical and longitudinal target coordinates are plotted, using the high-resolution front-end chamber information, together with the software cuts used to reject glass-related events. From the vertical traceback we have confirmed our assumption that the beam does not interact with the cylindrical glass sidewalls. The longitudinal (along the beam direction) traceback shows clearly the two ends caps of the cell, the bulk ^{3}He gas inside and the small pickup coil on the upstream side. The gates on the horizontal traceback spectra were placed to avoid the tails from the end-cap peaks and rejected $\approx 70\%$ of the data on tape. Presence of further background was checked with an empty cell and was found to be negligible.

The hardware trigger accepted events whenever one of the right-hand side scintillators fired in coincidence with the MRS. The subset of data in which one of the veto scintillators fired was ascribed to low-energy protons, while those events with hits in one of the thick scintillators, but no hits in the veto scintillators, were ascribed to neutrons. A hit in a scintillator was defined to be valid if the energy deposit was above threshold and the time-of-flight signal was below the time-out peak. In Fig. 5 the energy deposit versus time of flight for both veto and thick scintillators for the ^{3}He($p,2p$) subset is shown. The consistency of the data is apparent from the rising slope of the time of flight in the vetos with increasing energy loss, as one would expect for particles passing through the detector (lower-energy deposit for faster particles), and from the opposite slope in the thick scintillator, which is consistent with particles stopped in the scintillator. Matching of ADC and TDC signals for all the 16 bars was done by adding appropriate offsets to each individual scintillator, and a software cut was imposed on the

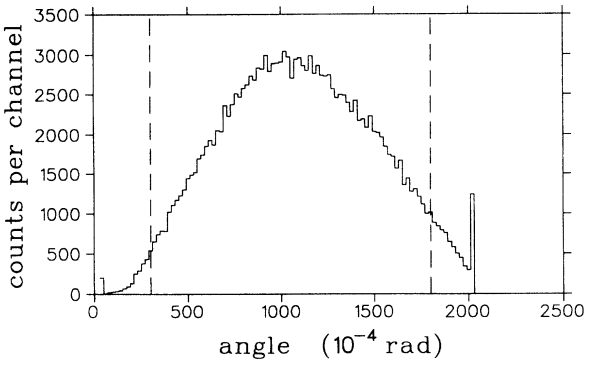

FIG. 3. Focal plane angle in the bend plane, corrected for the particle momentum, and the applied software cut.

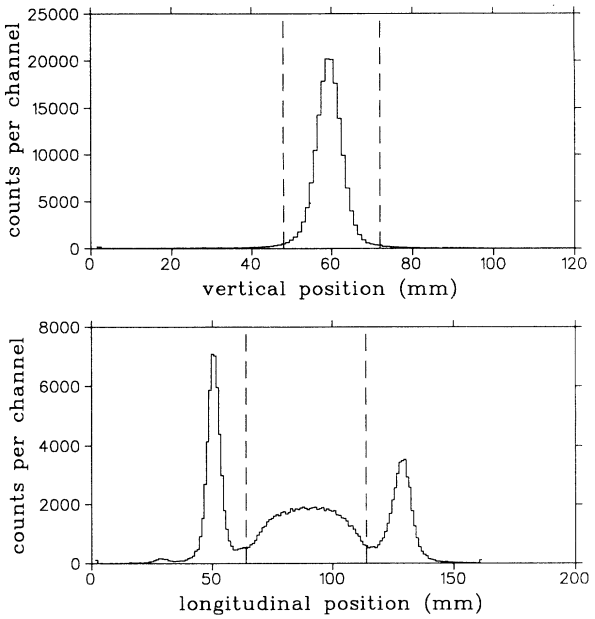

FIG. 4. Vertical (top) and longitudinal (bottom) ray tracing of the leading MRS protons back to the target and the software cuts imposed.

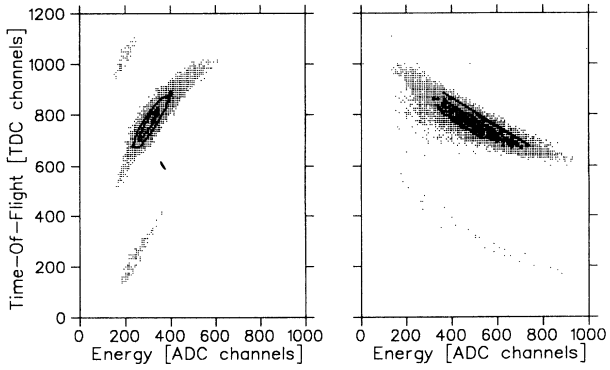

FIG. 5. Time of flight versus energy deposited in the vetos (left) and thick scintillators (right), for protons at 58°. The satellites in the spectra are from random events and from adjacent beam pulses (43-nsec separation).

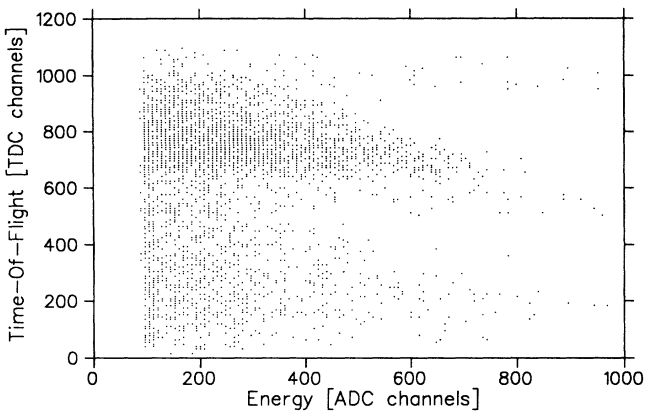

FIG. 6. Time of flight versus energy deposit in the scintillator bars for neutrons at 58°.

ADC signals just above the threshold.

For neutrons the procedure was somewhat different, since the energy deposit is not sharply defined as for the protons because of the different underlying mechanisms that produce the scintillation light. In the energy region of interest ($E_n = 50-120$ MeV), inelastic reactions on carbon dominate over elastic scattering from hydrogen [10]. At a threshold of 2 MeV electron equivalent, the efficiency $\eta(\omega)$ of the scintillators used (C:H ratio = 1:1) is estimated to be $20\% > \eta > 12\%$ [10]. The veto scintillator was thin enough (0.6 cm) that the neutron efficiency was $< 1\%$; hence, a neutron signature was a hit in the thick bar with no hit in the veto. In Fig. 6 the energy deposit versus time of flight for the thick scintillators for the ^{3}He(p,pn) subset is shown. One can see that the slower neutrons (longer time of flight) have a well-defined upper limit of energy deposit, but that the sharp structure of Fig. 5 is smeared out.

Combining the left and right information (leading protons in the MRS and low-energy nucleons in the scintillation array), the kinematic correlation between the two emitted nucleons could be clearly seen, as shown in Fig. 7. The time-of-flight spectra in the bottom figure is projected for a narrow bin of the focal plane coordinate corresponding to $80.8 < \omega < 87.5$ MeV. These spectra show the background level for the neutron and proton at the conjugate angle (58°) and for the proton at the nonconjugate angle (71°). Statistics for the ^{3}He(p,pn) reaction away from the quasifree peak (the 71° arm) were too low to make analysis of the data worthwhile. The time-of-flight resolution does not allow the separation of the ^{3}He($p,2p$) events into the two final-state channels, i.e., the deuterium ground state and the d^* spin singlet unbound state, although the structure of the peak shows a definite "shoulder" on the high side. The relative magnitude be-

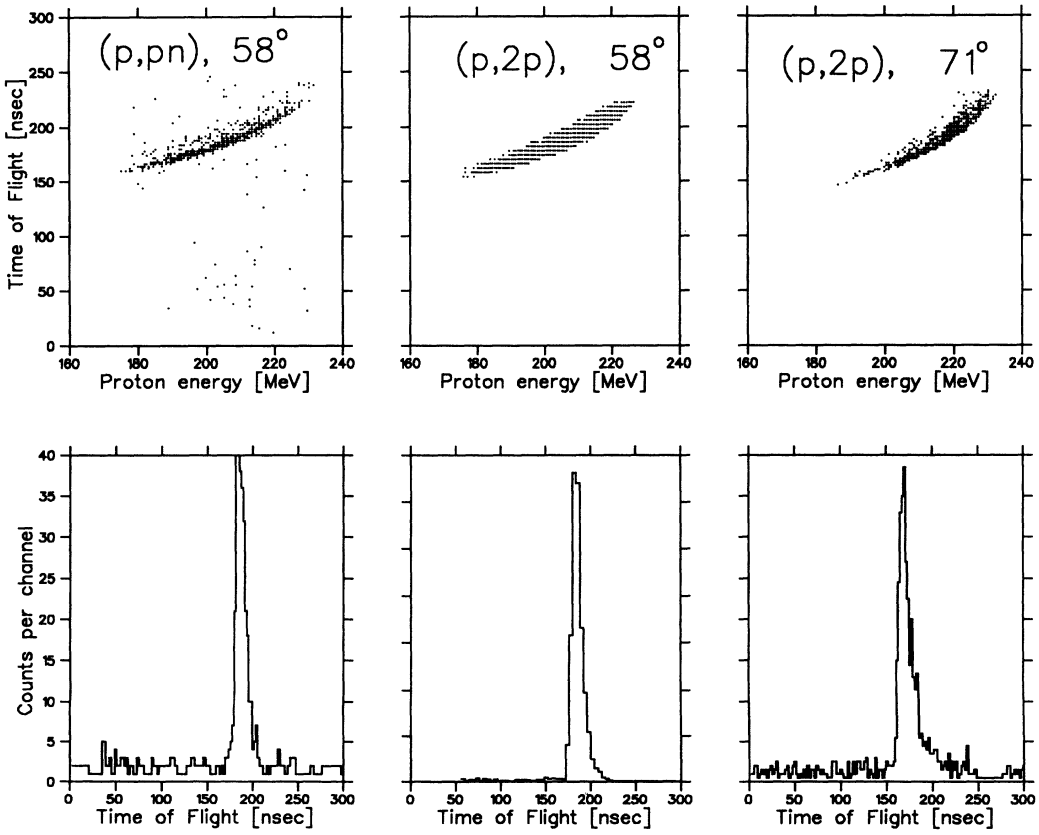

FIG. 7. Focal plane coordinate (momentum) of the leading proton in the MRS versus time of flight of the low-energy secondary nucleon (top). Time-of-flight projection for a narrow focal plane coordinate bin (bottom).

tween the d peak and the assumed d^* "shoulder" is consistent with earlier measurements [7] and with the expected triplet/singlet ratio of 3:1. The background on both sides of the peak is shown to be relatively low and uniform ("flat").

In order to test the validity of the neutron data and to ascertain that no protons leaked through the veto, a CH_2 target was used. The ratio of neutron events to proton events for the 58° array was observed to drop drastically, from 8.8% to 0.16%, which is consistent with the expected background. This test, however, does not cover the full area of the veto scintillators. The horizontal acceptance of 3.2° for the MRS corresponds to a 3.5° spread for the recoil protons, whereas the bars covered a horizontal angle of 7.1°. Thus veto inefficiencies at the edges would not be checked by this test.

Defining ω as the energy transfer to the knocked-out nucleon, we used the relation $\omega = E_b - E_{LP}$, where E_b is the incoming beam energy and E_{LP} the energy of the leading proton. The last quantity was calculated from the MRS focal plane coordinate, using the known MRS parameters [15]. Energy-loss corrections for the incident and scattered protons were applied. The relevant domain of ω (dictated by the spectrometer's acceptance) was $50 \leq \omega \leq 120$ MeV, and this region was subdivided into 16 bins. Events were accumulated for each bin separately, and consequently each run produced six yields (protons/neutrons in three beam polarization states) for each of the ω bins. The yield was defined to be the number of hits in the peak area (see Fig. 7, bottom) above the flat background. The accumulation of yields for each ω bin and polarization state was the input to the calculation of the spin observables, using Eq. (7) with s and S_A representing the actual polarization states of beam and target.

The small amount of N_2 atoms in the target (about 4%) amounts to 28% of the total number of nucleons. Although N_2 is expected to be unpolarized it can affect the measured polarization observables through its contribution to the measured cross section [Eq. (7)]. A dedicated measurement with a N_2-filled cell (2340 Torr at 273 K) confirmed that the contribution to the ^{3}He cross section at the particular geometries chosen is less than 4%. The reason for this small percentage is the surface character

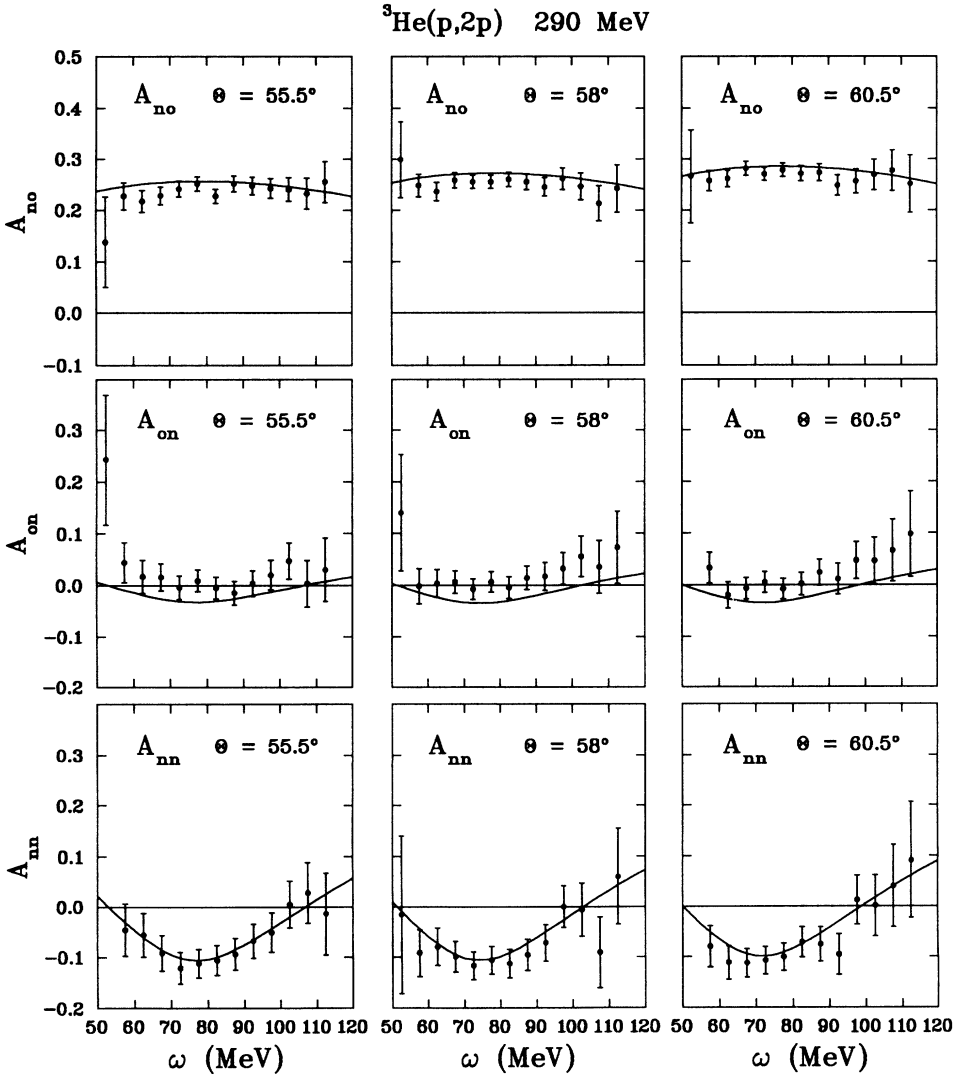

FIG. 8. Spin observables for the ^{3}He(p,2p) reaction and the left scintillator array (conjugate angle).

of the proton-induced reaction, the peaking of the spectral function for knockout from the $1p$ shell at higher nucleon momenta, and to differences in the appropriate missing-mass windows for $A=3$ and 14 target nuclei. Corrections of the spin observables for the effects of N_2 background were made and contributed negligibly to the total errors.

B. Detection efficiency, live time, and beam parameters

Several correction factors were applied to normalize the yields. The efficiency of the MRS wire chambers, i.e., the fraction of good to total events for each individual run, was 77% throughout the experiment. Events in which one of the wire chamber planes did not fire or registered a multiple hit were considered as inefficient events, and correspondingly the inefficiency was defined to be the ratio of those rejected events to the total candidates. The live time of the system was determined with an adjustable pulser which triggered the system at a rate proportional to the beam intensity, and the ratio between the accepted pulse events and the total pulser signals was taken as the live time. The live time varied during the experiment from 30% to 70%, depending on beam conditions, and each run was normalized accordingly.

The beam current was monitored by both the In-Beam Polarimeter [16] (IBP) and the Secondary Electron Emission Monitor (SEM), and the total flux and beam polarization were calculated using the IBP information. Total flux was corrected for accidental hits in both left and right polarimeter arms. Beam polarization was calculated from the IBP information using the known analyzing power A_y of 290-MeV protons in CH_2 ($A_y=0.378$) [16].

C. Extraction of spin observables

Using Eq. (7) with the four possible spin combinations for beam and target, the following relations hold for each of the ω bins:

$$\begin{aligned} Y_{\uparrow\uparrow} &= Y_0(1+P_{\uparrow}^b A_{n0}+P_{\uparrow}^t A_{0n}+P_{\uparrow}^b P_{\uparrow}^t A_{nn}) , \\ Y_{\uparrow\downarrow} &= Y_0(1+P_{\uparrow}^b A_{n0}-P_{\downarrow}^t A_{0n}-P_{\uparrow}^b P_{\downarrow}^t A_{nn}) , \\ Y_{\downarrow\uparrow} &= Y_0(1-P_{\downarrow}^b A_{n0}+P_{\uparrow}^t A_{0n}-P_{\downarrow}^b P_{\uparrow}^t A_{nn}) , \\ U_{\downarrow\downarrow} &= Y_0(1-P_{\downarrow}^b A_{n0}-P_{\downarrow}^t A_{0n}+P_{\downarrow}^b P_{\downarrow}^t A_{nn}) , \end{aligned} \tag{8}$$

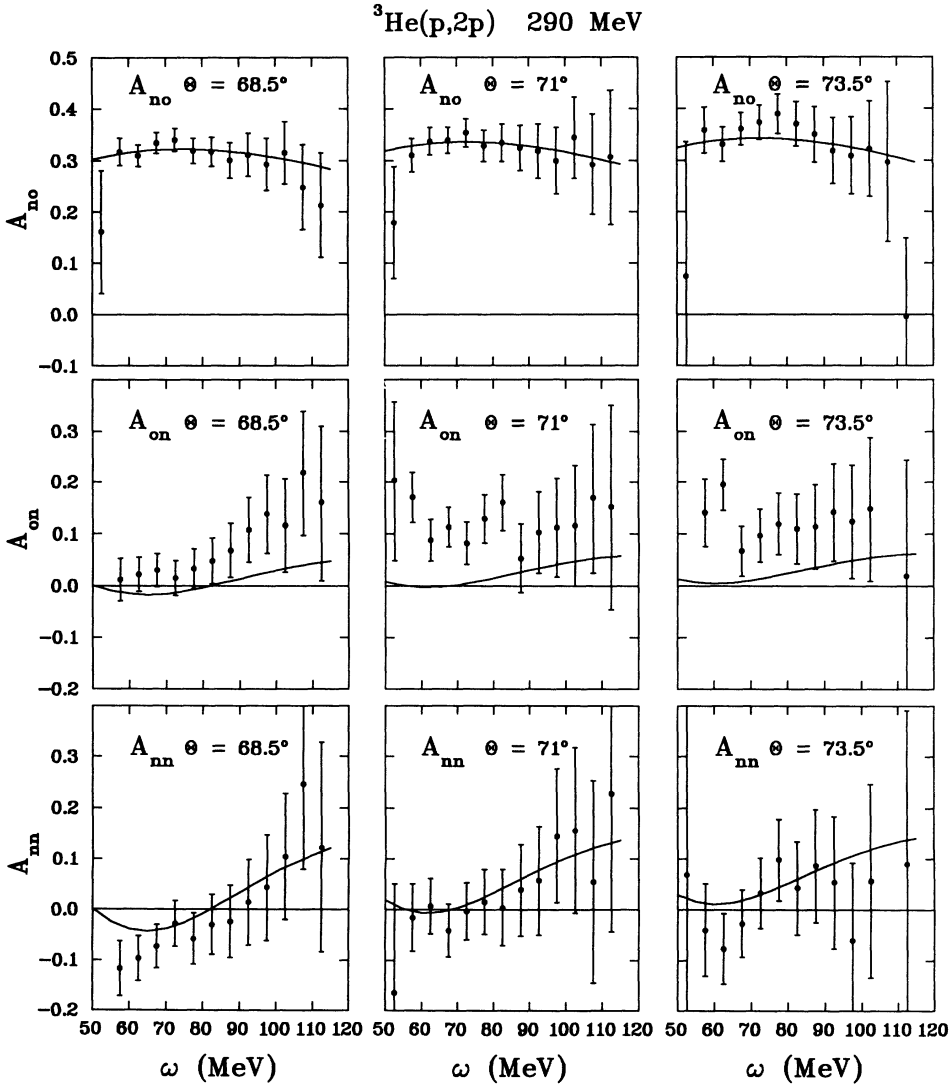

FIG. 9. Spin observables for the ^{3}He(p,2p) reaction and the right scintillator array (nonconjugate angle).

TABLE I. Beam-related spin observable (A_{n0}), ^{3}He(p,2p).

ω \ Θ	55.5°	58°	60.5°	68.5°	71°	73.5°
57.5 MeV	0.22±0.02	0.24±0.02	0.25±0.02	0.31±0.02	0.31±0.03	0.35±0.04
62.5 MeV	0.21±0.02	0.23±0.01	0.26±0.01	0.31±0.02	0.33±0.02	0.33±0.03
67.5 MeV	0.22±0.01	0.25±0.01	0.28±0.01	0.33±0.02	0.33±0.02	0.36±0.03
72.5 MeV	0.24±0.01	0.25±0.01	0.27±0.01	0.34±0.02	0.35±0.02	0.37±0.03
77.5 MeV	0.25±0.01	0.25±0.01	0.27±0.01	0.31±0.02	0.32±0.03	0.38±0.03
82.5 MeV	0.22±0.01	0.26±0.01	0.27±0.01	0.31±0.02	0.33±0.03	0.37±0.04
87.5 MeV	0.25±0.01	0.25±0.01	0.27±0.01	0.30±0.03	0.32±0.04	0.35±0.05
92.5 MeV	0.24±0.01	0.24±0.01	0.24±0.02	0.31±0.04	0.31±0.05	0.31±0.06
97.5 MeV	0.24±0.01	0.26±0.02	0.25±0.02	0.29±0.05	0.29±0.06	0.30±0.07
102.5 MeV	0.24±0.02	0.24±0.02	0.26±0.03	0.31±0.06	0.34±0.07	0.32±0.09
107.5 MeV	0.23±0.03	0.21±0.03	0.27±0.04	0.24±0.08	0.29±0.09	0.29±0.15
112.5 MeV	0.25±0.04	0.24±0.04	0.25±0.05	0.21±0.10	0.30±0.13	

where Y_{bt} denotes the measured normalized yield for the respective spin states of beam and target, P^b and P^t are the measured beam and target polarizations (absolute values), Y_0 is proportional to the unpolarized cross section (arbitrary units), and A_{bt} are the usual spin observables. The above equations can therefore be solved exactly to obtain the four unknown parameters Y_0, A_{n0}, A_{0n}, and A_{nn}. However, the multitude of runs with different polarization values ($\approx$150 analyzable runs) created an overdetermined system of equations which had to be solved numerically to give the best fit to the four-parameter function [Eq. (8)]. This was done using the CERN library software package MINUIT [17], a program which minimizes a χ^2 multiparameter function and performs shape and error analysis. The procedure outlined above was repeated for each ω bin for both ^{3}He(p,2p) and ^{3}He(p,pn) reactions. The final results will be discussed in the next section.

V. RESULTS AND DISCUSSION

A. ^{3}He(p,2p) reaction

The results for the ^{3}He(p,2p) reaction are shown in Fig. 8 and 9, where the scattering angle Θ represents the central angle of the relevant veto scintillator. The left scintillator array (Fig. 8) was centered around the conjugate two-body angle (58°), and the right array was centered around the nonconjugate angle (71°). Solid lines represent the PWIA calculations described in Sec. II. The errors accounted for both statistical errors and the quality of the χ^2 minimization. In Tables I–III the three spin observables are tabulated for each angle and ω bin.

Some insight into the underlying reaction mechanism is gained by observing the dependence of the spin observables on the momentum transfer to the residual nucleus (i.e., the momentum of the struck nucleon in the PWIA; see Fig. 10). As the projection of the (ω,Θ) plane onto the $|q|$ axis causes some overlap of data points with the same $|q|$ value, but on different sides of the conjugate angle, this mapping is not unique. While the A_{n0} observable (both data and PWIA predictions) is a multivalued function of $|q|$ for the ^{3}He(p,2p) reaction, the results for A_{n0} and A_{nn} appear to lie on a single-valued smooth function of $|q|$. This is caused by the exact pairing of protons spins (i.e., $D_{SS'}$ independent of S) predicted by the PWIA to occur for a specific proton momentum $q_0 \approx 80$ MeV/c.

The differential spin-average cross sections σ_0 from the χ^2 minimization are shown in Fig. 11. The solid line

TABLE II. Target-related spin observable (A_{0n}), ^{3}He(p,2p).

ω \ Θ	55.5°	58°	60.5°	68.5°	71°	73.5°
57.5 MeV	0.04±0.03	0.00±0.03	0.03±0.03	0.01±0.04	0.17±0.04	0.14±0.06
62.5 MeV	0.01±0.03	0.00±0.02	−0.02±0.02	0.02±0.03	0.08±0.04	0.19±0.05
67.5 MeV	0.01±0.02	0.00±0.02	0.00±0.02	0.03±0.03	0.11±0.03	0.06±0.04
72.5 MeV	0.00±0.02	0.00±0.02	0.00±0.02	0.01±0.03	0.08±0.04	0.09±0.05
77.5 MeV	0.00±0.02	0.00±0.02	0.00±0.02	0.03±0.03	0.12±0.04	0.11±0.05
82.5 MeV	0.00±0.02	0.00±0.02	0.00±0.02	0.04±0.04	0.16±0.05	0.11±0.06
87.5 MeV	−0.01±0.02	0.01±0.02	0.02±0.02	0.06±0.05	0.05±0.06	0.11±0.08
92.5 MeV	0.00±0.02	0.01±0.02	0.01±0.03	0.10±0.06	0.10±0.07	0.14±0.09
97.5 MeV	0.02±0.02	0.03±0.03	0.04±0.03	0.13±0.07	0.11±0.09	0.12±0.10
102.5 MeV	0.04±0.03	0.05±0.03	0.04±0.04	0.11±0.09	0.11±0.11	0.14±0.13
107.5 MeV	0.00±0.04	0.03±0.05	0.06±0.06	0.21±0.12	0.16±0.14	−0.47±0.20
112.5 MeV	0.03±0.06	0.07±0.07	0.09±0.08	0.16±0.15	0.15±0.19	0.01±0.22

TABLE III. Mixed spin observable (A_{nn}), ^{3}He(p,2p).

ω \ Θ	55.5°	58°	60.5°	68.5°	71°	73.5°
57.5 MeV	−0.04±0.05	−0.09±0.04	−0.08±0.04	−0.11±0.05	−0.01±0.06	−0.04±0.09
62.5 MeV	−0.05±0.04	−0.08±0.03	−0.11±0.03	−0.09±0.04	0.00±0.05	−0.07±0.07
67.5 MeV	−0.09±0.03	−0.09±0.03	−0.11±0.02	−0.07±0.04	−0.04±0.05	−0.02±0.06
72.5 MeV	−0.12±0.03	−0.11±0.02	−0.10±0.02	−0.02±0.04	0.00±0.05	0.03±0.06
77.5 MeV	−0.11±0.02	−0.10±0.02	−0.10±0.02	−0.05±0.05	0.01±0.06	0.09±0.08
82.5 MeV	−0.10±0.02	−0.11±0.02	−0.07±0.03	−0.03±0.05	0.00±0.07	0.04±0.09
87.5 MeV	−0.09±0.03	−0.09±0.03	−0.07±0.03	−0.02±0.07	0.03±0.09	0.08±0.11
92.5 MeV	−0.06±0.03	−0.07±0.03	−0.09±0.04	0.01±0.08	0.05±0.10	0.05±0.13
97.5 MeV	−0.05±0.03	0.00±0.04	0.01±0.04	0.04±0.10	0.14±0.13	−0.06±0.15
102.5 MeV	0.00±0.04	0.00±0.05	0.00±0.06	0.10±0.12	0.15±0.16	0.05±0.19
107.5 MeV	0.02±0.06	−0.09±0.07	0.04±0.08	0.24±0.16	0.05±0.19	−0.22±0.31
112.5 MeV	−0.01±0.08	0.06±0.09	0.09±0.11	0.12±0.20	0.22±0.27	0.08±0.30

shows the PWIA predictions for the conjugate scattering angle (58°), while the dashed line shows the predictions for the nonconjugate angle (71°). The data for the two respective angles were corrected for the MRS acceptance and contain an undetermined normalization factor. The momentum-density distribution $\rho(q)=\frac{1}{2}\sum_S D^{SS'}(q)$ was extracted from the differential cross section and is shown in Fig. 12. The agreement with the PWIA is within the experimental errors for both the conjugate and nonconjugate arrays.

The data are seen to agree with PWIA theory within experimental errors for the A_{n0} and A_{nn} observables (see Figs. 8 and 9). The beam-related analyzing power A_{n0} is close to the value for free pp scattering [$A_{n0}(pp)\sim 0.29$] and depends very weakly on the momentum of the struck nucleon. The target-related analyzing power A_{0n} is expected to be small, first, because A_{0n} in pp scattering is rather small [$A_{0n}(pp)\sim 0.29$], and, second, because of the spin-momentum distributions of protons in ^{3}He. The A_{0n} data are systematically above the predicted curves. Repeated replays of the data have shown that the relatively small shift of ≈ 0.03 in the 58° data might be an instrumental effect related to the infrequent flip of the target polarization (4–6 h between AFP target-spin reversals). However, the deviations are larger for the 71° data which disagree substantially with the PWIA. In contrast to this, data on the spin-correlation parameter A_{nn} of Fig. 10 are much less sensitive to the normalization of target spin up/down runs. If the PWIA calculations are taken at face value, one may deduce that the two protons are spin saturated [$D^{SS'}_{\text{proton}}(q)$ is independent of S] at $|q_0|\approx 80$ MeV/c, where A_{nn} vanishes. Error analysis of Eq. (8) shows that this observable is about 4 times less sensitive to instrumental effects affecting spin up/down normalizations, and furthermore the sensitivity to spin-momentum distributions is three times as large. Several different replays have confirmed the excellent stability of

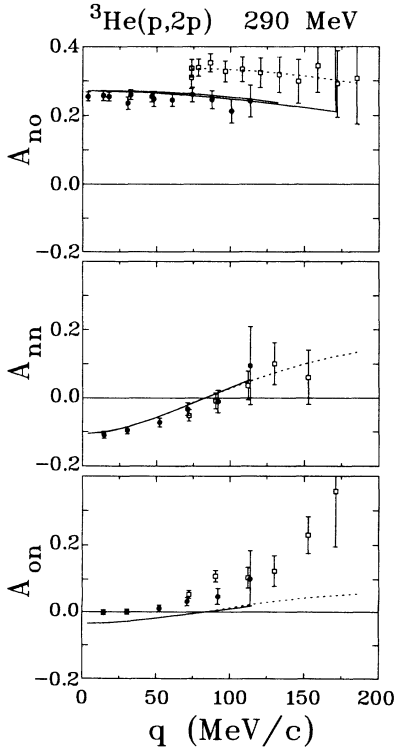

FIG. 10. Spin observables for the ^{3}He(p,2p) reaction as a function of the momentum of the struck proton.

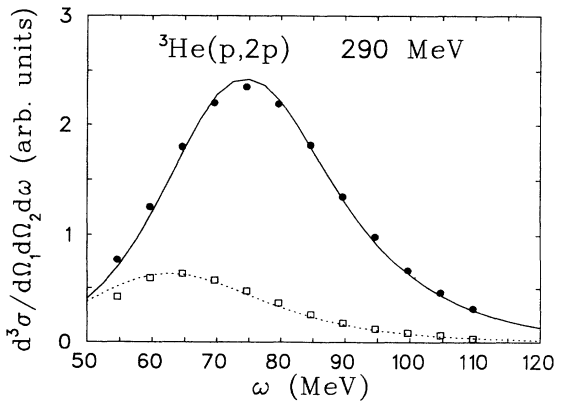

FIG. 11. Differential cross section for the ^{3}He(p,2p) reaction. The data have been multiplied by a single arbitrary normalization factor.

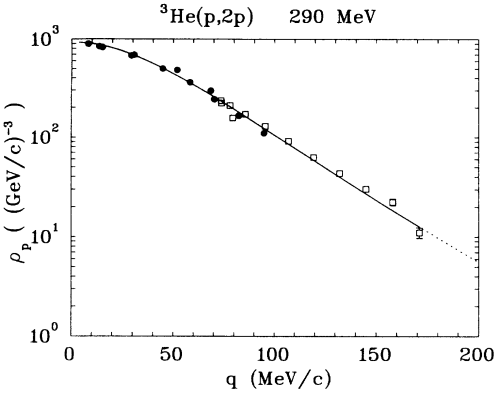

FIG. 12. Momentum-density distribution $\rho_p(q)$ vs the momentum of the struck proton. The experimental data have been multiplied by a single arbitrary normalization factor.

the A_{nn} data. At momenta q, where data from both arrays overlap, the results agree well and have been averaged. The $(p,2p)$ A_{nn} results differ strongly from those for pp scattering [$A_{nn}(pp)\sim 0.82$] and reflect the spin-momentum distribution of the protons in ^{3}He. At $q=0$ the protons are favored to be antiparallel to the ^{3}He spin. This is in good agreement with the calculations which, furthermore, show that the spin-momentum correlation effects are predominantly caused by the weak mixed-symmetry S' states. Our measurement could be interpreted as evidence that the S' states contribute about 1.5% to the ^{3}He wave function, in agreement with Faddeev calculations, e.g., those of Afnan and Birrell [4]. These tentative conclusions could become firm provided future explicit calculations of final-state interaction effects would show that these effects are small.

In general, the proton knockout data are in fair agreement with the PWIA predictions. Previous work [6,7] reported some deviations from the PWIA at low momentum transfer, and the disagreements of A_{0n} are another indication that rescattering corrections are not altogether negligible for the $(p,2p)$ reaction.

B. ^{3}He(p,pn) reaction

The expected cross section for the ^{3}He(p,pn) reaction should be lower than the ^{3}He$(p,2p)$ cross section by a factor of 3, based on the NN cross section and on the ratio of nucleons in the target. Furthermore, knocked-out neutrons from the ^{3}He(p,pn) reaction are detected with much lower efficiency than the protons; hence, the statistical errors are much larger. The rate of ^{3}He(p,pn) events was within the expected neutron detection efficiency in

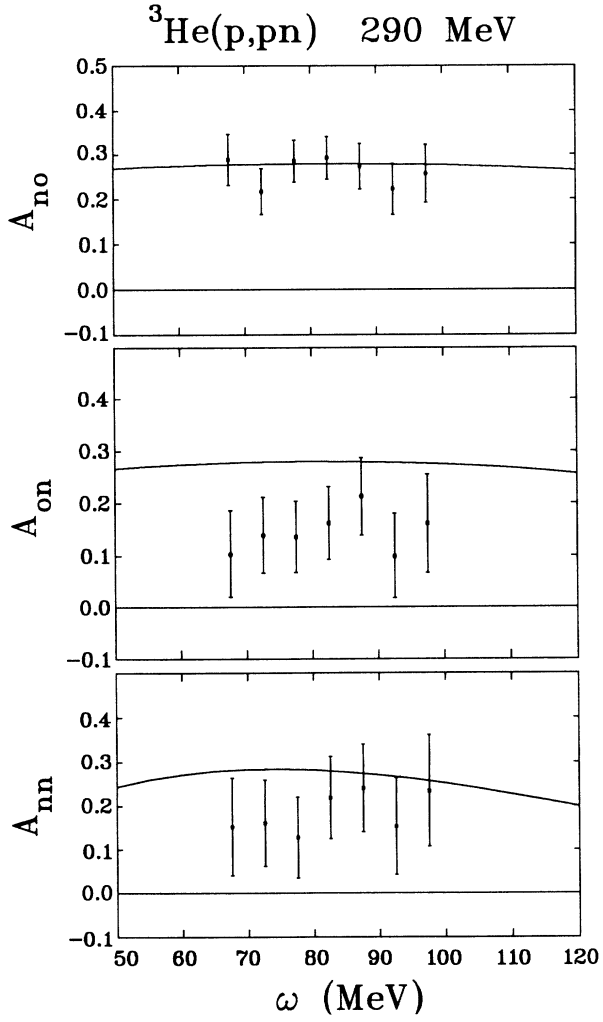

FIG. 13. Spin observables for the ^{3}He(p,pn) reaction and the left scintillator array (conjugate angle).

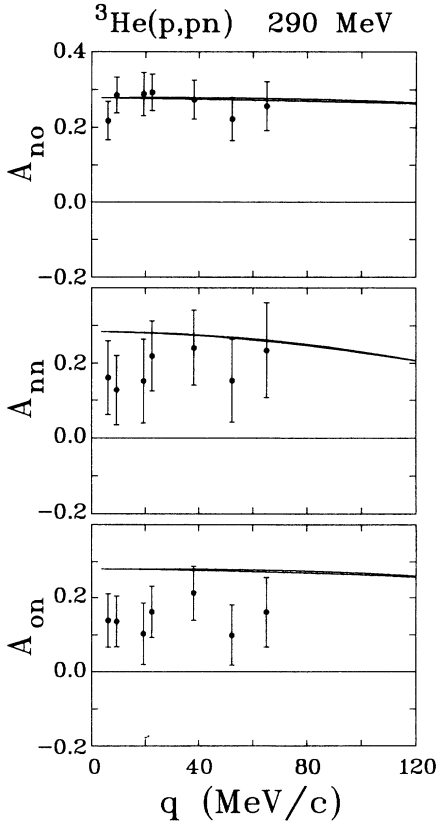

FIG. 14. Spin observables for the ^{3}He(p,pn) reaction as a function of the momentum of the struck neutron.

this energy range (15%–20%). This situation made the extraction of physical quantities from the right-hand scintillation array (the nonconjugate angle) statistically unreliable, and consequently we will present results for the left-side (conjugate angle) array only.

In Fig. 13 the extracted spin observables for the conjugate angle (58°) are shown. Events from the three veto scintillators in this array have been summed to improve the statistical accuracy. While the A_{n0} observable is in good agreement with the PWIA predictions, there is a marked deviation of the A_{0n} and A_{nn} observables which is not explained within this model. This deviation indicates a breakdown of the PWIA, which is in marked contrast with the proton data. The discrepancy could also be explained by an instrumental effect (proton leakthrough of a few percent), although a check of a fraction of the area in the conjugate array using *PP* scattering showed no evidence for this effect. The behavior of these observables was tested over different subsets of the measured data set and was found to be below the theoretical predictions in a consistent way, although with some variations attributed to the higher statistical errors. The dependence of these observables on the momentum transfer q to the residual nucleus is shown in Fig. 14.

C. Conclusions

The measurements reported here represent the first nucleon knockout results from a polarized target with $A>2$. The ^{3}He$(p,2p)$ data for A_{nn} are drastically different from those for free *PP* scattering. They are predicted by the PWIA to be sensitive to the spin-momentum distributions of protons in ^{3}He. The good quantitative agreement between the data and PWIA suggests that, for this particular observable in $(p,2p)$ knockout, rescattering effects are likely to be small. The mixed symmetry S' component in the ^{3}He wave function ($\approx 1.5\%$ suggested by Faddeev calculations), produces a characteristic q dependence of A_{nn}, which is observed experimentally. The present measurements may then be interpreted as confirming its existence at qualitatively the expected magnitude. Spin saturation, i.e., $D^{SS'}_{\text{proton}}(q)$ independent of S, was observed to occur at proton momenta $|q_0| \approx 80$ MeV/c, again in agreement with the PWIA predictions. The exact value of q_0 will depend on the magnitude of final-state interaction effects. The small shifts for the A_{0n} observable are an indication that rescattering effects are not altogether negligible in $(p,2p)$ knockout.

The large deviations from the PWIA predictions of the A_{0n} spin observable, and also of the A_{nn} observable, in neutron knockout are presently not understood. Additional theoretical and experimental effort is required to investigate this difference. The $(p,2p)$ final state is dominated ($\approx 75\%$) by the deuteron bound state, whereas for the (p,pn) reaction the two protons in the final state are in a free-scattering state. This basic difference may imply that rescattering corrections are more important in the (p,pn) reaction. Furthermore, the $(p,2p)$ reaction is 3 times more likely than the (p,pn) reaction and this may make neutron knockout more vulnerable to rescattering corrections. A new experiment with much better counting statistics and at an incident energy of 220 MeV has recently been carried out [18] specifically to investigate the importance of rescattering in the ^{3}He(p,pn) reaction.

If rescattering is confirmed to be important in neutron knockout, this result may also have implications for the interpretation of measurements of the electric form factor of the neutron in quasielastic scattering from polarized ^{3}He (see Ref. [3]). Recent calculations by Laget [19] of polarization observables for the reaction $^3\vec{\text{He}}(\vec{e},e'n)pp$ predict rescattering effects due to final-state interactions and meson-exchange currents to be significant at the low-momentum transfers [$Q^2<0.2$ (GeV/c)^2] relevant for the present experiment. Particularly large effects are predicted for the target-related asymmetry in the direction normal to the scattering plane (A_{0n} in the present notation, A_Y^0 in Ref. [19]), which vanishes in the PWIA for $(e,e'N)$ reactions. Unfortunately, there are no experimental data to test these calculations. In contrast to this situation, the (p,pn) reaction studied in the present work exhibits significant deviations from the PWIA; however, calculations of final-state interaction effects have yet to be performed.

This work was supported by grants from the Natural Sciences and Engineering Research Council of Canada.

[1] O. Häusser, J. Phys. (Paris) Colloq. **51**, C6-99 (1990); A. Rahav *et al.*, Phys. Lett. B **275**, 259 (1992).
[2] J. L. Friar, B. F. Gibson, G. L. Payne, A. M. Bernstein, and T. E. Chupp, Phys. Rev. C **42**, 2310 (1991), and references therein.
[3] C. E. Woodward *et al.*, Phys. Rev. Lett. **65**, 698 (1990); A. K. Thompson *et al.*, report, 1992.
[4] I. R. Afnan and N. D. Birrell, Phys. Rev. C **16**, 823 (1977).
[5] R. A. Arndt and L. D. Roper, Scattering Analysis Interactive Dial-in (SAID) program (unpublished).
[6] M. B. Epstein *et al.*, Phys. Rev. C **32**, 967 (1985).
[7] E. Jans *et al.*, Nucl. Phys. **A475**, 687 (1987).
[8] G. Jacob and Th. A. J. Maris, Rev. Mod. Phys. **38**, 121 (1966).
[9] B. Blankleider and R. M. Woloshyn, Phys. Rev. C **29**, 538 (1984).
[10] R. A. Cecil, B. D. Anderson, and R. Madey, Nucl. Instrum. Methods **161**, 439 (1979).
[11] B. Larson, O. Häusser, P. P. J. Delheij, D. M. Whittal, and D. Thiessen, Phys. Rev. A **44**, 3108 (1991).
[12] T. E. Chupp, M. Wagshul, K. P. Coulter, A. B. McDonald, and W. Happer, Phys. Rev. C **36**, 2244 (1987), and references therein.
[13] O. Häusser, in *Spin and Isospin in Nuclear Reactions,* Proceedings of the Telluride Conference, edited by S. W. Wissiuk (Plenum, New York, 1991), p. 381.
[14] G. G. Ohlsen, Rep. Prog. Phys. **35**, 717 (1972), and references therein.
[15] O. Häusser, computer program MRS (unpublished).
[16] R. Abegg and R. Schubank, TRIUMF design note TRI-DN-87-17,1987.
[17] F. James and M. Roos, CERN Computer program library, D506 (unpublished).
[18] TRIUMF experiment E616; E. Brash *et al.* (unpublished).
[19] J. M. Laget, Phys. Lett. B **273**, 367 (1991).

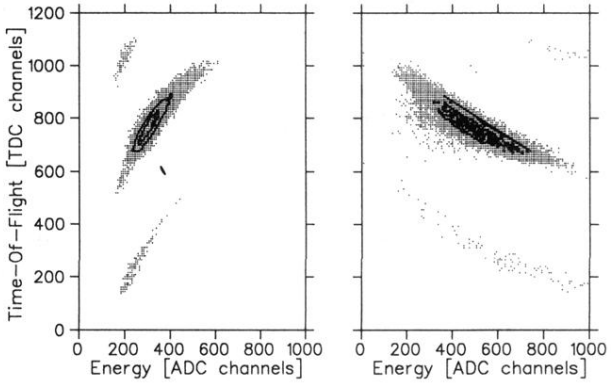

FIG. 5. Time of flight versus energy deposited in the vetos (left) and thick scintillators (right), for protons at 58°. The satellites in the spectra are from random events and from adjacent beam pulses (43-nsec separation).